frontiers | Frontiers in Marine Science

TYPE Original Research
PUBLISHED 29 July 2024
DOI 10.3389/fmars.2024.1444302

OPEN ACCESS

EDITED BY
Wilson Machado,
Fluminense Federal University, Brazil

REVIEWED BY
Zhang Yuanbiao,
State Oceanic Administration, China
Luiz Drude Lacerda,
Federal University of Ceara, Brazil

*CORRESPONDENCE
Lumin Sun
sunlumin@xmu.edu.cn

RECEIVED 06 June 2024
ACCEPTED 12 July 2024
PUBLISHED 29 July 2024

CITATION
You X, Sun L, Chen X, Li Y, Zheng J, Yuan D, Wu J and Sun S (2024) Mercury distribution and transfer in mangrove forests in urban areas under simulated rising sea levels. *Front. Mar. Sci.* 11:1444302. doi: 10.3389/fmars.2024.1444302

Mercury distribution and transfer in mangrove forests in urban areas under simulated rising sea levels

Xilin You[1,2], Lumin Sun[1]*, Xiaozheng Chen[1,2], Yiting Li[2], Jue Zheng[1,2], Dongxing Yuan[2], Junjie Wu[1,2] and Shiyu Sun[1]

[1]Key Laboratory of Estuarine Ecological Security and Environmental Health, Education Department of Fujian, Tan Kah Kee College, Xiamen University, Zhangzhou, China, [2]State Key Laboratory of Marine Environmental Science, Xiamen University, Xiamen, China

This study assesses the impact of simulated sea level rise (SLR) on mercury distribution and migration in an urban mangrove wetland on the northern coast of Maluan Bay, Xiamen City, Fujian Province, China. Two adjacent Kandelia obovata mangrove plots with elevations representing current sea level and a 40-cm SLR were examined. Total mercury (THg), methylmercury (MeHg), and mercury isotopes in sediments from different elevations were analyzed to reveal the geochemical behavior of mercury under a simulated 100-year SLR scenario. THg and MeHg distribution in sediments mirrored patterns of biogenic elements (carbon, nitrogen, and phosphorus), suggesting adsorption onto organic matter as the primary entry mechanism. Low-elevation plots showed significantly higher concentrations of THg, MeHg, total organic carbon (TOC), total nitrogen (TN), and total phosphorus (TP) compared to high-elevation plots. Mercury isotope characteristics indicated that the primary mercury source was anthropogenic emissions from surrounding lands, entering the wetland from both landward and seaward directions. The study highlights the crucial role of mangrove wetlands in mercury pollution control and nutrient cycling under SLR conditions. Results suggest that SLR enhances the retention capacity of mangrove wetlands for THg, MeHg, and nutrients. This research provides a scientific basis for mangrove conservation and restoration, offering new insights into the geochemical behavior of mercury in vegetated intertidal ecosystems in the context of climate change.

KEYWORDS

mercury distribution, mangrove wetlands, sea level rise (SLR), methyl mercury (MeHg), mercury isotopes, biogenic elements

1 Introduction

Mercury (Hg), one of the most toxic heavy metals occurring naturally, considerably threatens environmental health. In recent years, its high toxicity and global distribution have received increased attention (Amos et al., 2013; Beckers and Rinklebe, 2017; Al Sulaiti et al., 2022). Although Hg emissions may be limited to specific areas, long-distance transportation results in contamination even in remote locations (Gonzalez Raymat et al., 2017; Dastoor et al., 2022). Upon entering an ecosystem, inorganic Hg (II) undergoes a biomethylation facilitated by microorganisms in soil and water, resulting in the formation of the toxic methylmercury (MeHg) (Ma et al., 2019; Regnell and Watras, 2019; Feng et al., 2022). Via bioaccumulation and biomagnification, MeHg seriously threatens human health and the ecosystem (Liu et al., 2019; Tang et al., 2020; Ye et al., 2021).

Wetlands are particularly sensitive to Hg contamination (Poulin et al., 2019; Neal Walthall et al., 2022). The input-output mass balances of Hg in wetlands are complex (Zillioux et al., 1993; Fitzgerald et al., 2007). On the one hand, the abundant organic matter in wetlands can absorb Hg from runoff, making it an important natural Hg sink (Thompson Roberts and Pick, 2000; Poulin et al., 2019). On the other hand, the output of Hg into wetlands can be enhanced by various environmental factors (Bergamaschi et al., 2012a; de Lacerda et al., 2020; Selvendiran et al., 2008). Moreover, wetlands can act as both sources and sinks of MeHg (Tjerngren et al., 2012; Johnson et al., 2016). The evapor-transpiration of terrestrial vegetation can affect the Hg flux between surface soils and the atmosphere (Poulain et al., 2007; Ariya et al., 2015), and Hg in the atmosphere is deposited onto leaf surfaces and enters the leaf tissues through foliar stomata during gas exchange (Luo et al., 2016; Wang et al., 2022), reaching the soil via litterfall (Teixeira et al., 2017, 2018; Wang et al., 2021). Furthermore, vegetation can effectively limit Hg exchange between land and the atmosphere by directly absorbing Hg released from the land surface into the atmosphere, and by impeding the upward diffusion of atmospheric Hg, thereby increasing the deposition rate of Hg from the atmosphere (Obrist et al., 2012). Therefore, vegetation growth and coverage are important factors affecting the accumulation and transformation of Hg in wetlands (Ye et al., 2020).

Mangroves are typical warm-temperate intertidal wetland systems with high primary productivity (Kristensen et al., 2008). Because of their location, mangrove forests function as a key intermediary area for Hg translocation among marine, freshwater, and terrestrial environments and have a great Hg accumulation potential (Castro et al., 2021). In mangrove wetlands, Hg is predominantly stored in sediment in the forms of dissolved organic Hg and particulate Hg, and it exhibits a certain degree of mobility (Lei et al., 2019; de Lacerda et al., 2020). Mercury present in sediments has the potential to be re-introduced into nearby bodies of water or the atmosphere through tidal action (Bergamaschi et al., 2012b), volatilization, and uptake by plant roots, as demonstrated by studies conducted in tidal environments such as Lagoon (Bouchet et al., 2011) and sawgrass wetlands (Meng et al., 2018). Research has shown that substantial amounts of dissolved organic Hg in mangroves can be released into the water during dry periods, while particulate Hg is primarily transported to the nearshore marine environment during periods of heavy rainfall (de Lacerda et al., 2022). Abundant sulfate and organic matter levels and active microbial communities make mangrove sediments an excellent platform for the microbially mediated methylation of inorganic Hg (Correia and Guimaraes, 2017; Duan et al., 2021).

With accelerated urbanization and industrialization, mangrove wetlands surrounding coastal cities are at increased risk of Hg contamination. Consequently, the migratory behavior of Hg in mangrove wetlands adjacent to densely populated regions is anticipated to become more pronounced (Bergamaschi et al., 2012b; Duan et al., 2021).

Mercury isotopic compositions have been widely used as valuable tracers and indicators in the determination of Hg origin, transfer, and destination in various environmental systems since the application of the multi-collector inductively coupled plasma mass spectrometer (MC-ICP-MS) (Bergquist and Blum, 2007; Yin et al., 2014). Because Hg from different sources can be characterized by mass-dependent fractionation (MDF) and mass-independent fractionation (MIF), the use of a two-dimensional system of isotopic signatures to examine the biogeochemical process of Hg in mangrove wetlands is justified (Sun et al., 2017). Although studies in this field are scarce, river runoff, surrounding seawater, and atmospheric deposition are the main external Hg sources of mangrove forests, and the Hg from seawater accounts for approximately 40% (Araujo et al., 2017; Huang et al., 2020). Most Hg is subjected to photo reduction before entering the wetlands (Huang et al., 2022). More than half of the Hg in plant roots is derived from sediments, and nearly 90% if the Hg in leaf tissues originates from the atmosphere (Sun et al., 2017). The reduction of Hg (II) by natural organic matter has been observed in mangrove tissues (Huang et al., 2022), and tidal activity can also affect biochemical Hg transformation in mangrove wetlands (Huang et al., 2020).

Sea level rise (SLR) is one of the critical negative consequences of global warming (Dutton et al., 2015). As typical intertidal wetlands, mangrove ecosystems are considerably subjected to submergence (Saintilan et al., 2020). Recently, several studies showed that SLR caused different degrees of changes in the functions and structures of mangrove ecosystems, such as physiological tolerance, seedling biomass, species composition, biomass accumulation, and organic carbon stocks (Woodroffe, 1995; Lovelock and Ellison, 2007; Albert et al., 2017; Chen et al., 2020). Similarly, Hg distribution and migration in mangrove wetlands could be affected by SLR. However, the relevant features and processes are still not well known. In the present study, the levels of total Hg, methylmercury, and Hg stable isotopes in the sediments from two connected *Kandelia obovata* mangrove forests under different intertidal elevations were determined. The aims of this work were to define the variation of Hg storage in the sediments under different simulated sea levels and to clarify the effects of SLR on Hg migration in mangrove wetlands. The results provide a scientific basis for the assessment of the geochemical behavior of Hg in vegetated intertidal ecosystems in the context of global warming.

2 Materials and methods

2.1 Field site

The targeted mangrove forest (118.0344°E, 24.5526°N) is situated along the northern coastline of Maluan Bay in Xiamen, Fujian, China (Figure 1). This area experiences a subtropical monsoon climate, with an annual air temperature ranging from 3.8°C to 36.1°C, approximately 2,270 hours of sunshine, and over 1,000 mm of precipitation annually. The seawater salinity in this location ranges from 26 to 30 psu, with a tidal range of 4 m for the local semidiurnal tide (Chen et al., 2020). Furthermore, there are multiple mangrove forests located within a 30-km radius of this region.

The study site, originally abandoned crab ponds, was subjected to mangrove restoration in 2004. For this purpose, soil and sediment from the ponds were used to facilitate the growth of mangroves, with Kandelia obovata and Avicennia marina species being planted in the same year. By 2014, Kandelia obovata had emerged as the predominant species in the area (Chen et al., 2020, 2022). The sampling area consisted of two adjacent woodlands (sites SLR 40 cm and SLR 0 cm) with varying elevations, namely 375 and 415 cm, respectively, compared to the local mean sea level of 365 cm. And the mean inundation times were 8 h/d and 6 h/d (i.e., 5 h, 4 h and 3 h per tide) at Sites SLR 40 cm and SLR 0 cm, respectively (Chen and Ye, 2014). Based on the findings of Chen et al. (2022) indicating an average sea level rise rate of 3.3 mm per year in China between 1980 and 2018, a vertical difference of 40 cm between the two locations was employed to model the anticipated SLR of approximately 100 years for mangrove forests within the same vicinity and adjacent areas.

2.2 Sample collection and preparation

In April 2018, six sediment core samples were collected during low tide from S1 to S6, respectively (Figure 1). Each core sample was then sliced into 5 subsections at 8-cm intervals. The samples were placed in polyethylene Ziplock bags, stored in an icebox, and transported to the laboratory (Duan et al., 2021; Sun et al., 2017). Upon arrival, the sediment samples were individually lyophilized, ground with an agate mortar, sieved with a 200-mesh nylon screen, packaged in double plastic Ziplock bags, and preserved at -4°C for subsequent analysis (Huang et al., 2020).

2.3 Total mercury (THg) and MeHg analysis

For the analysis of THg, the sediment samples were digested in a mixed acid solution of nitric acid and sulfuric acid at a ratio of 7:3 (v/v) overnight at 70°C. Following digestion, the solution was diluted and treated with bromine chloride before analysis. The Hg in the sample solution was then sequentially reduced using hydroxylamine hydrochloride and tin chloride solutions, purged with Hg-free argon gas, and concentrated in gold traps. The trapped Hg was thermally released using a dual-trap amalgamation system and carried by Hg-free argon gas into a cold vapor atomic fluorescence spectrometer (AF-610D, Beijing Ruili, China) for quantification (USEPA, 2002).

In the analysis of MeHg, each powder sample underwent initial extraction with a 25% KCl-methanol solution at 60°C for 5 hours. The resulting extraction solution was then distilled, and the distillates were collected in a PFA (polyfluoroalkoxy) receiver in an ice bath, using ultra-pure water. These distillates were subsequently transferred to a PFA sampling bottle and ethylated with $NaBEt_4$. Finally, the ethylated Hg species were analyzed using an automated alkyl Hg analytical system (MERXTM, Brooks Rand Labs, USA) as described in previous studies (Duan et al., 2021; USEPA, 2001).

Standard solutions (10 ng·L^{-1} THg, diluted from the original standard solution of NIST 3133) and two certified reference materials for sediment (GBW08308 for THg and ERM-CC580 for MeHg) were subjected to analysis alongside the samples for quality

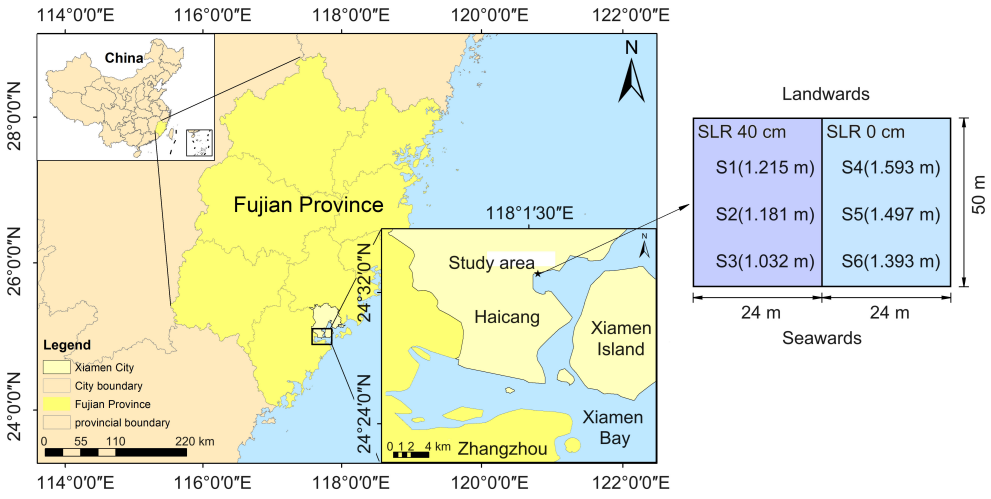

FIGURE 1
Location of the study area and sampling sites.

control. The standard solution exhibited a value of 9.7 ± 0.8 ng·L^{-1} (n = 3, 1SD), and the measured THg value of GBW08308 and the MeHg value of ERM-CC580 were 465 ± 18 ng·g^{-1} THg (n = 3, 1SD) and 69.85 ± 6.13 ng·g^{-1} MeHg (n = 3, 1SD), respectively. These values closely approximated the certified reference values of 480 ± 30 ng·g^{-1} THg (recovery of 94% to 104%) and 75 ± 4 ng·g^{-1} MeHg (recovery of 84% to 103%), respectively. The correlation coefficients (R^2) for the fit of the calibration curves were > 0.997 and > 0.993 for THg and MeHg, respectively, meeting the requirements of this study.

2.4 Mercury isotopic composition analysis

The isotopic compositions of Hg were analyzed using a multi-collector inductively coupled plasma mass spectrometer (Nu Instruments Ltd. UK) equipped with a DSN-100 desolvating nebulizer (Nu Instruments, Wrexham, U.K.) and an in-house cold vapor generation device (Lin et al., 2015). The analytical procedure for Hg isotopes was developed in the laboratory following established methodologies (Bergquist and Blum, 2007; Lin et al., 2015). Thallium standards (NIST SRM 997) and a Hg sample-standard (NIST SRM 3133) were used as internal and bracketing standards, respectively.

Reference materials NIST SRM 8610 and DORM-4 were used for quality control purposes. To achieve analytical concentrations exceeding 1 ng·mL^{-1}, the Hg in selected samples required concentration via a purged-trap method prior to analysis (Sun et al., 2017) (See details in Supplementary Material). The measured values for δ^{202}Hg and Δ^{199}Hg were -0.58 ± 0.13‰ and 0.03 ± 0.04‰ for NIST SRM 8610 (2 SD, n = 12) and 0.42 ± 0.03‰ and 1.76 ± 0.11‰ for DORM-4 (2 SD, n = 2), respectively, aligning with the findings of previous studies (Bergquist and Blum, 2007; Huang et al., 2020; Sun et al., 2017). All vessels used in this study were constructed from borosilicate glass or PTFE, and the cleaning procedure adhered to USEPA method 1631, Revision E.

2.5 Biogenic elemental analysis

In the sediment, total nitrogen (TN) was quantified using an elemental analyzer (Vario EL Cube, Elementar, Germany), and total phosphorus (TP) was assessed through ammonium molybdate colorimetry following sample digestion with alkaline potassium persulfate (Zhao et al., 2022). The total organic carbon (TOC) content in the sediment samples was determined using a total organic carbon analyzer (TOC-LCPH, Shimadu, Japan). The geographical coordinates of the sampling sites were obtained in the field using a satellite differential real-time kinematic system (RTK-G10A, UniStrong, China).

2.6 Statistical analysis

Normal distribution testing was performed to analyze all data, and the results are presented as means ± standard deviation (SD). The *Pearson* test and the *Wilcoxon signed-rank* test were employed to evaluate the correlation and significance of differences among various parameters at different elevations. Furthermore, bivariate and multiple linear regressions were performed using the SPSS 22.0 statistics package (SPSS Inc. USA).

3 Results

3.1 Spatial characteristics of biogenic elements

The graphs presented in Figure 2 and Supplementary Figure S1 illustrate the recorded levels of TOC, TN, and TP in the collected samples. The TOC content ranged from 1.16% to 2.26%, with an average of 1.50 ± 0.32% (n = 30, 1SD). Additionally, the concentrations of TOC were lower at the seaward (mean 1.42 ± 0.22% for S3 & S6, n = 10, 1SD) compared to the landward (mean 1.64 ± 0.34% for S1 & S4, n = 10, 1SD, $p < 0.05$). Furthermore, a vertical analysis revealed a decrease in the TOC content from the superficial layer (mean 1.73 ± 0.22 for depth of 0–8 cm and 1.85 ± 0.27 for depth of 8–16 cm, 1 SD) to the deep layer mean (1.37 ± 0.19 for depth of 24–32 cm and 1.28 ± 0.06 for depth of 32–40 cm, n = 6, 1 SD) ($p < 0.05$). There is no significant difference in the profile distribution of TOC in sediment between the SLR 40 cm site and the SLR 0 cm site.

The total nitrogen content in sediments ranged from 0.49 to 1.39 g·kg^{-1}, with a mean value of 0.88 ± 0.25% (n = 30, 1SD). A gradual decrease in total nitrogen was observed from the landward side (mean 0.97 ± 0.27 g·kg^{-1}, for sampling sites S1 & S4) to the seaward side (0.82 ± 0.24 g·kg^{-1}, for sampling sites S3 & S6) ($p \leq 0.05$). Furthermore, the surface layer (1.00 ± 0.24 for a depth of 0–8 cm, n = 6, 1SD) exhibited higher total nitrogen levels compared to the deep layers (0.76 ± 0.15 for a depth of 10–20 cm and 0.78 ± 0.16 for a depth of 32–40 cm, n = 6, 1SD) ($p < 0.05$). Additionally, the total nitrogen profile distribution at the SLR 40 cm site was significantly greater than that at the SLR 0 cm site ($p < 0.05$).

The concentrations of TP in sediment samples varied from 0.16 to 0.41 g·kg^{-1}, with an average of 0.25 ± 0.07% (n = 30, 1 SD), indicating statistically significant differences in horizontal distribution ($p \leq 0.05$). Specifically, the landward side (0.19 ± 0.03 g·kg^{-1}, for S1 & S4, n = 10, 1SD) exhibited a lower TP content than the seaward side (0.27 ± 0.07 g·kg^{-1}, for S3 & S6, n = 10, 1SD). However, no significant difference in the TP content was observed across different depths in the vertical profile. Furthermore, similar to the total nitrogen (TN) levels, the TP content at the SLR 40 cm site was significantly higher than that at the SLR 0 cm site ($p < 0.05$).

The C/N ratio serves as a crucial indicator of the origin of organic materials and, subsequently, for the allocation of sediment sources. In this study, the C/N ratios ranged from 11.81 to 27.79, with a mean value of 17.75 ± 3.94 (n = 30, 1SD). The C/N values of SLR 40 cm site (mean value of 16.61 ± 0.46, n=15, 1SD) were significantly lower than those of SLR 0 cm site (mean value of 18.76 ± 1.22, n=15, 1SD) ($p < 0.05$). However, no significant differences were found in the vertical and horizontal distribution of C/N values among the sampling sites.

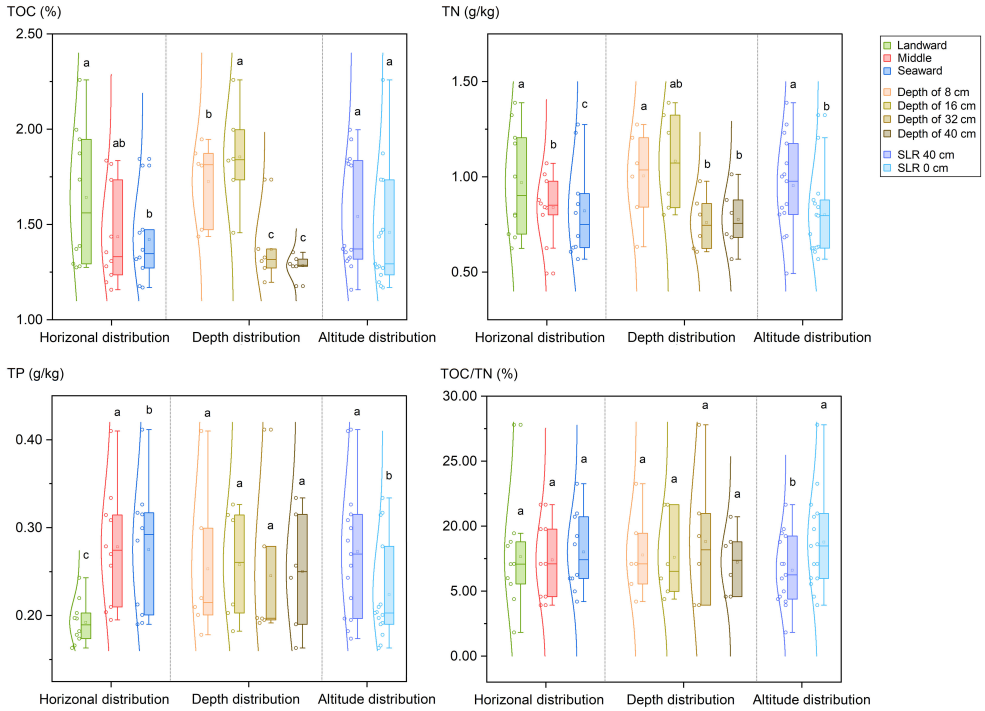

FIGURE 2
Distribution of total organic carbon (TOC), total nitrogen (TN) content and total phosphorus (TP) in sediments of planted *K. obovata* forests. Different lowercase letters denote statistically significant differences between groups (p<0.05).

3.2 Mercury concentrations and isotopic ratios

Data on the concentrations of THg and MeHg as well as the isotopic mercury compositions are presented in Table 1 and Supplementary Figure S2. On average, the THg concentrations were 42.4 ± 28.1 ng·g^{-1} (n = 30, 1SD), with a range from 19.5 to 134.5 ng·g^{-1}. As shown in Figure 3A, the THg levels were notably elevated on both the landward side (54.6 ± 34.0 ng·g^{-1}, for S1 & S4, n = 10, 1SD) and the seaward side (38.3 ± 15.8 ng·g^{-1}, for S3 & S6, n = 10, 1SD) compared to the middle zone (34.3 ± 9.3 ng·g^{-1}, for S2 & S5, n = 10, 1SD) ($p < 0.05$). Vertical distribution patterns revealed a

TABLE 1 Summary of measured mercury results of the sediment samples from Zengying mangrove wetland (n=30, 1SD).

Sample site	Depth (cm)	THg (ng·g^{-1})	MeHg (ng·g^{-1})	δ^{202}Hg (‰)	Δ^{199}Hg (‰)	Δ^{200}Hg (‰)	Δ^{201}Hg (‰)
S1	8	57.4 ± 1.4	0.22 ± 0.04	−1.35 ± 0.06	−0.14 ± 0.01	0.00 ± 0.01	−0.17 ± 0.03
	16	134.5 ± 16.1	0.25 ± 0.01	−0.22 ± 0.06	−0.08 ± 0.01	0.00 ± 0.01	−0.07 ± 0.03
	24	40.6 ± 1.9	0.25 ± 0.03	−1.90 ± 0.06	−0.16 ± 0.01	−0.01 ± 0.01	−0.17 ± 0.03
	32	48.3 ± 2.8	0.13 ± 0.01	−1.44 ± 0.06	−0.12 ± 0.01	0.01 ± 0.01	−0.14 ± 0.03
	40	35.5 ± 2.2	0.17 ± 0.01	−1.31 ± 0.06	−0.14 ± 0.01	−0.01 ± 0.01	−0.17 ± 0.03
S2	8	45.2 ± 5.0	0.16 ± 0.01	−1.41 ± 0.06	−0.13 ± 0.01	0.02 ± 0.01	−0.17 ± 0.03
	16	44.4 ± 3.2	0.05 ± 0.01	−1.28 ± 0.06	−0.16 ± 0.01	−0.01 ± 0.01	−0.15 ± 0.03
	24	23.8 ± 2.4	0.10 ± 0.01	−1.35 ± 0.06	−0.15 ± 0.01	0.01 ± 0.01	−0.16 ± 0.03
	32	38.0 ± 2.7	0.24 ± 0.01	−1.14 ± 0.06	−0.16 ± 0.01	−0.01 ± 0.01	−0.18 ± 0.03
	40	27.7 ± 1.5	0.12 ± 0.02	−1.02 ± 0.06	−0.12 ± 0.01	0.01 ± 0.01	−0.15 ± 0.03
S3	8	50.7 ± 2.2	0.11 ± 0.01	−1.58 ± 0.06	−0.16 ± 0.01	−0.01 ± 0.01	−0.15 ± 0.03
	16	54.4 ± 1.5	0.30 ± 0.02	−1.65 ± 0.06	−0.15 ± 0.01	0.00 ± 0.01	−0.18 ± 0.03

(Continued)

TABLE 1 Continued

Sample site	Depth (cm)	THg (ng·g^{-1})	MeHg (ng·g^{-1})	δ^{202}Hg (‰)	Δ^{199}Hg (‰)	Δ^{200}Hg (‰)	Δ^{201}Hg (‰)
	24	21.2 ± 0.8	0.10 ± 0.01	−1.37 ± 0.06	−0.11 ± 0.01	0.02 ± 0.01	−0.15 ± 0.03
	32	31.6 ± 2.2	0.13 ± 0.01	−1.37 ± 0.06	−0.10 ± 0.01	0.01 ± 0.01	−0.15 ± 0.03
	40	29.4 ± 2.1	0.08 ± 0.01	−1.51 ± 0.06	−0.14 ± 0.01	0.02 ± 0.01	−0.17 ± 0.03
S4	8	37.5 ± 1.8	0.06 ± 0.01	−1.45 ± 0.06	−0.09 ± 0.01	0.02 ± 0.01	−0.13 ± 0.03
	16	102.3 ± 7.9	0.20 ± 0.01	−0.53 ± 0.06	−0.06 ± 0.01	0.01 ± 0.01	−0.04 ± 0.03
	24	37.0 ± 1.4	0.10 ± 0.01	−1.51 ± 0.06	−0.19 ± 0.01	0.00 ± 0.01	−0.19 ± 0.03
	32	33.1 ± 2.7	0.15 ± 0.00	−0.90 ± 0.06	−0.15 ± 0.01	0.00 ± 0.01	−0.17 ± 0.03
	40	19.5 ± 0.8	0.10 ± 0.00	−1.35 ± 0.06	−0.14 ± 0.01	0.02 ± 0.01	−0.18 ± 0.03
S5	8	39.8 ± 2.8	0.09 ± 0.01	−1.31 ± 0.06	−0.12 ± 0.01	−0.01 ± 0.01	−0.15 ± 0.03
	16	48.0 ± 3.4	0.17 ± 0.02	−1.15 ± 0.06	−0.16 ± 0.01	−0.01 ± 0.01	−0.14 ± 0.03
	24	23.7 ± 3.6	0.02 ± 0.00	−1.25 ± 0.06	−0.11 ± 0.01	−0.01 ± 0.01	−0.16 ± 0.03
	32	30.4 ± 2.6	0.18 ± 0.01	−1.26 ± 0.06	−0.13 ± 0.01	0.02 ± 0.01	−0.14 ± 0.03
	40	22.5 ± 2.7	0.08 ± 0.00	−0.96 ± 0.06	−0.12 ± 0.01	0.01 ± 0.01	−0.16 ± 0.03
S6	8	74.7 ± 3.9	0.24 ± 0.04	−1.66 ± 0.06	−0.15 ± 0.01	0.00 ± 0.01	−0.16 ± 0.03
	16	30.3 ± 4.3	0.10 ± 0.00	−1.50 ± 0.06	−0.17 ± 0.01	0.01 ± 0.01	−0.21 ± 0.03
	24	22.5 ± 0.6	0.05 ± 0.01	−1.36 ± 0.06	−0.13 ± 0.01	0.00 ± 0.01	−0.12 ± 0.03
	32	35.5 ± 4.4	0.13 ± 0.03	−1.50 ± 0.06	−0.14 ± 0.01	0.02 ± 0.01	−0.16 ± 0.03
	40	32.6 ± 1.7	0.15 ± 0.03	−1.19 ± 0.06	−0.14 ± 0.01	−0.01 ± 0.01	−0.14 ± 0.03

higher THg content in the upper and middle sediment layers (mean 50.9 ± 13.7 ng·g^{-1} for a depth of 0–8 cm and 68.9 ± 40.4 ng·g^{-1} for a depth of 8–16 cm, n = 6, 1SD) compared to the lower layer (mean 36.1 ± 6.5 ng·g^{-1} for a depth of 24–32 cm and 27.9 ± 6.0 ng·g^{-1} for a depth of 32–40 cm, n = 6, 1SD) ($p < 0.05$). Furthermore, the SRL 40 cm site exhibited a significantly higher overall THg content compared to the SRL 0 cm site ($p < 0.05$).

The mean concentration of MeHg was 0.14 ± 0.07 ng·g^{-1} (n = 30, 1SD), ranging from 0.02 to 0.30 ng·g^{-1}. A significant positive correlation was observed between MeHg and THg (*Pearson*'s r = 0.5872, $p < 0.01$). However, there was no significant difference in the MeHg content between sediments from the landward side (0.16 ± 0.06 ng·g^{-1}, for S1 & S4, n = 10, 1SD) and the seaward side (0.14 ± 0.07 ng·g^{-1}, for S3 & S6, n = 10, 1SD) as well as between shallow surface sediments (mean 0.15 ± 0.07 ng·g^{-1} for a depth of 0–8 cm and 0.18 ± 0.09 ng·g^{-1} for a depth of 8–16 cm, n = 6, 1SD) and deeper sediments (mean 0.16 ± 0.04 ng·g^{-1} for a depth of 15–20 cm and 0.12 ± 0.04 ng·g^{-1} for a depth of 32–40 cm, n = 6, 1SD).

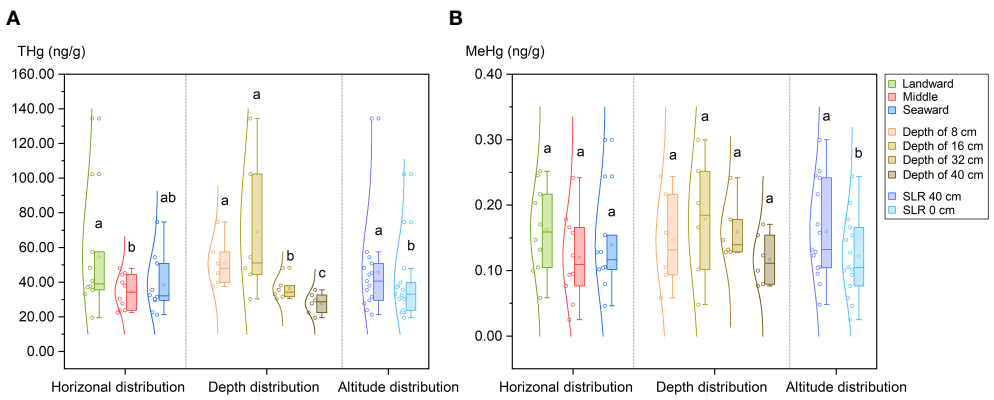

FIGURE 3
Mercury distribution in sediments of planted *K. obovata* forests. **(A)** Distribution of total mercury (THg); **(B)** Distribution of methyl mercury (MeHg). Different lowercase letters denote statistically significant differences between groups (p<0.05).

Conversely, the MeHg content in the SLR 40 cm site (0.16 ± 0.03 $ng{\cdot}g^{-1}$) was significantly higher than that in the SLR 0 cm site (0.12 ± 0.03 $ng{\cdot}g^{-1}$) ($p < 0.05$), consistent with the pattern observed for THg (Figure 3B).

The MeHg/THg ratio, a metric used to assess the methylation potential of Hg in sediment samples (Yu et al., 2021), ranged from 0.11% to 0.63%, with a mean value of 0.36 ± 0.15% (n = 30, 1SD). Notably, the MeHg/THg ratio in surface sediments (mean 0.28 ± 0.09% at a depth of 0–8 cm) was significantly lower than that in deeper sediments (mean 0.42 ± 0.09% at a depth of 32–40 cm) ($p < 0.05$). However, there were no significant differences in the horizontal distribution of the MeHg/THg ratio in sediments or among sites with different elevations.

The isotopic mean values of δ^{202}Hg, Δ^{199}Hg, Δ^{200}Hg, and Δ^{201}Hg were -1.29 ± 0.38‰, -0.13 ± 0.03‰, 0.00 ± 0.01‰, and -0.15 ± 0.04‰ (n = 30), respectively, with corresponding ranges of -1.90 to -0.22‰, -0.19 to -0.06‰, -0.01 to 0.02‰, and -0.21 to -0.04‰. There were no significant differences in the MDF or MIF of Hg between horizontal and vertical distributions. However, a significant difference was observed in the Δ^{201}Hg values between the two sites at varying elevations, with the SLR 40 cm site displaying lower Δ^{201}Hg values compared to the SLR 0 cm site ($p < 0.05$).

Pearson's correlation analysis (Supplementary Table S1) showed that δ^{202}Hg was significantly correlated with THg (r = 0.532), Δ^{199}Hg (r = 0.585), and Δ^{201}Hg (r = 0.704), Δ^{199}Hg was significantly correlated with THg (r = 0.386) and Δ^{201}Hg (r = 0.741), and Δ^{201}Hg was also significantly correlated with THg (r = 0.672).

4 Discussion

4.1 Mercury distribution

The THg concentrations in the collected sediments were lower than those observed for mangrove sediments heavily impacted by industrial emissions (typically exceeding 100 $ng{\cdot}g^{-1}$) (Chai et al., 2020) but comparable to the background values (55 $ng{\cdot}g^{-1}$) of mangrove sediments in adjacent regions (Cai et al., 2019) and pristine sites with minimal human activity (mean values ranging from 30.3 to 86 $ng{\cdot}g^{-1}$, Table 2). Similarly, the concentrations of MeHg in the sediment samples from the study area were low compared to previous findings (Table 2). Under natural conditions, most mangrove sediments show increasing THg levels with increasing depth, which can be attributed to the historical presence of significant Hg pollution in locations such as the Futian Bay of Shenzhen, Guangdong Province, China (Li et al., 2016), the Catuama Estuary in Northeast Brazil (Vilhena et al., 2013), the Cochin Estuary in Southwest India (Passos et al., 2022), and the Cubatao Estuary in Southeast Brazil (Castro et al., 2021). Additionally, light and temperature regimes can influence the release of Hg from the surface of intertidal zones into the atmosphere, whereas tidal action can result in the erosion of surface sediments in the intertidal zone, leading to lower THg concentrations compared to those of the deeper sediment layers (Huang et al., 2022). The study area has been artificially created through the deposition of marine sediments during a short period

TABLE 2 Comparison of THg and MeHg contents in mangrove sediments between this study and recent reports.

Location	Country	Year	Vegetation type	THg ($ng{\cdot}g^{-1}$)	MeHg ($ng{\cdot}g^{-1}$)	Depth (cm)	References
Zengying, Fujian province	China	2018	planted forest	42.4 ± 24.3	0.14 ± 0.07	0–40	This study
Zini, Fujian province	China	2018	natural forest	86 ± 24		0–50	Huang et al., 2020
Shatian, Guangxi province		2017		43 ± 27			
Mawei, Guangxi province	China	2017	natural forest	141 ± 68		0–25	Huang et al., 2022
Dafeng, Guangxi province	China	2017	natural forest	65.4 ± 3.8	0.12 ± 0.01	0–20	Duan et al., 2021
Jinhai, Guangxi province				54.4 ± 2.5	0.17 ± 0.01		
Dongzhai, Hainan province				159 ± 9.1	0.46 ± 0.03		
Xinying, Hainan province				86.1 ± 3.9	0.26 ± 0.02		
Yunxiao, Fujian province				64.9 ± 3.3	0.18 ± 0.02		
				117 ± 7.1	0.37 ± 0.03		

(Continued)

TABLE 2 Continued

Location	Country	Year	Vegetation type	THg ($ng \cdot g^{-1}$)	MeHg ($ng \cdot g^{-1}$)	Depth (cm)	References
Futian, Guangdong province							
Baguang, Guangdong province	China	2016	natural forest	80.91		0–5	Chai et al., 2020
Shajing, Guangdong province				414.50			
Xixiang, Guangdong province				272.30			
Setiu, Terengganu	Malaysia	2017	natural forest	75.0 ± 6.9		0–2	Siau et al., 2021
Sundarban, Bangladesh	India	2015	natural forest	30.3 ± 8.3		0–5	Islam et al., 2017
Cubatao, São Paulo State	Brazil	2005	natural forest	128–2540		0–240	Castro et al., 2021
Campos Basin, Rio de Janeiro State	Brazil	2014	natural forest	82.5 ± 49.4	0.79 ± 0.52	0–2	Araujo et al., 2017

rather than through natural sedimentation processes. As a result, the distribution of elemental compounds at various depths within the study site is relatively homogeneous (Chen et al., 2020). Supplementary Figure S2 illustrates a decreasing trend in the THg content in the sediments with increasing depth, suggesting that surface sediments receive external Hg inputs compared to the less disturbed lower sediment layers. The elevated levels of THg in the landward and seaward sediments, compared to those in the middle zone, may be attributed to both external inputs of Hg from terrestrial and marine sources, as well as differences in microtopography and associated chemical processes during sedimentation. In the estuarine environment, organic matter, especially dissolved organic matter (DOM) represented by humic substances, can effectively bind with Hg, and the binding capacity is influenced by environmental factors such as salinity (Cavalcante et al., 2024). In this study, there was a strong positive correlation between the THg concentration in sediments and the TOC content ($r = 0.711$, $p < 0.01$), indicating that organic matter has a promoting effect on the enrichment of Hg.

Sediments play a crucial role as both a source and sink of MeHg, with local *in-situ* Hg methylation and external inputs serving as the primary contributors to MeHg levels (Mao et al., 2020). The unique characteristics of the mangrove ecosystem, including a high organic matter content, a low pH, anoxic conditions, and the presence of sulfate/sulfate-reducing bacteria, create an optimal environment for Hg methylation (Al Sulaiti et al., 2022). Whilst a strong positive correlation between MeHg and THg concentrations suggests that *in-situ* methylation is the predominant source of MeHg in the sediments of the study site, the low MeHg content showed no clear spatial distribution pattern.

The MeHg/THg ratio (0.36 ± 0.15%) falls within the lower range of the 0.1%–7% reported for coastal and marine sediments (Lei et al., 2019), aligning with the approximately 0.3% ratio observed in sediment samples collected from mangrove wetlands along the southeastern coast of China in 2017 (Duan et al., 2021). These results imply that the level of Hg methylation in the sediments of the study site is inadequate. Moreover, the absence of a significant correlation between the MeHg/THg ratio and the THg levels suggests that factors other than the concentration of THg, such as microorganisms and soil physicochemical properties, primarily influence the methylation process in the study area (Duan et al., 2021; Lei et al., 2019).

Sulfide-rich sediments have enhanced mercury methylation capabilities in comparison to other environments (Mikac et al., 1985). Furthermore, organic matter has been identified as a significant factor in microbially mediated Hg methylation in anoxic sediments (Navya et al., 2015). There is a strong association between the formation of MeHg and the presence of organic matter (Moreau et al., 2015), which may be attributed to the stimulating impact of organic matter on bacterial growth (da Silva et al., 2008). In environments abundant in organic matter, such as mangrove forests, the presence of sulfate-reducing bacteria and their associated biota can expedite Hg methylation (Guimaraes et al., 2000). The prolonged interaction between Hg and organic material results in an increased production of MeHg (De Pontes et al., 2023). Nevertheless, the levels of MeHg observed in the sampled sites showed no notable association with TOC. This discrepancy may be attributed to the diminished microbial activity in the artificially filled sampling sites compared to that in natural sediments (Lei et al., 2019).

4.2 Mercury transfer

Mercury isotopes are subjected to both MIF and MDF processes, each associated with specific transformation mechanisms. Of these, MIF is predominantly linked to photochemical reactions, whereas MDF can occur in any physicochemical process, including but not limited to biotic and dark redox transformations, even in sample preparation and isotope analysis (Bergquist and Blum, 2007). Notably, the distinct Hg isotopic signatures resulting from these processes can be applied to identify the sources of Hg deposition in sedimentary environments. Atmospheric Hg and terrestrial runoff display distinct MIF and MDF characteristics (Thibodeau and Bergquist, 2017). Sediments primarily impacted by atmospheric Hg(II) deposition generally exhibit elevated Δ^{199}Hg values (Gehrke et al., 2007), whereas those influenced by terrestrial sources tend to display slightly lower Δ^{199}Hg values and markedly more negative δ^{202}Hg signatures relative to atmospheric Hg^0 (Zhou et al., 2023).

The MDF in sediment vary as a result of alterations in Hg input sources or the introduction of novel fractionation mechanisms (Kurz et al., 2019), leading to an escalation in MDF levels attributed to anthropogenic influences (Yin et al., 2018). In pristine environments, where natural conditions remain largely intact, the δ^{202}Hg values in soil or sediment are typically lower (Wang et al., 2017; Liu et al., 2023). Conversely, regions close to urban and industrial emission sources demonstrate elevated δ^{202}Hg values in sedimentary Hg, indicative of a slightly negative trend (Estrade et al., 2011; Huang et al., 2020). Furthermore, samples significantly contaminated by direct anthropogenic Hg emissions exhibit Δ^{199}Hg values approaching zero (Bergquist and Blum, 2007). The sedimentary MDF and MIF values at the study site were negative. While the overall levels of THg in the sediments at the study sites are relatively low, there is a significant positive correlation between δ^{202}Hg and Δ^{199}Hg values and THg concentration. This indicates that the rise in THg levels may be attributed to potential Hg sources stemming from nearby human activities. Table 3 demonstrates that the δ^{202}Hg and Δ^{199}Hg values closely resemble the monitoring data from a mangrove wetland in an urban coastal area affected by industrial pollution (Blum et al., 2014; Huang et al., 2022). This indicates that the presence of Hg in the mangrove sediments is primarily attributed to the terrestrial input of anthropogenic Hg emissions, as opposed to atmospheric sources. Additionally, the MDF and MIF values in the sediments showed no statistically significant differences in either horizontal distribution from landward to seaward or vertical distribution from surface to deep layers, suggesting a similar pattern of Hg sources among the sampled sites. This also indicates that the spatial differences in the distribution of THg in the sediments are not related to the sources and biogeochemical processes of Hg but are more likely due to differences in microtopography or the geochemical deposition processes of Hg.

The ratios of Δ^{199}Hg/Δ^{201}Hg and Δ^{199}Hg/δ^{202}Hg are important indicators of the transfer and alteration Hg within the environment (Blum et al., 2014). For example, the Δ^{199}Hg/Δ^{201}Hg ratios of 1.36 ± 0.04 and 1.00 ± 0.01 correspond to the photodegradation and

TABLE 3 Comparison of mercury isotopic compositions in wetland sediments between this study and recent reports.

Location	Sample type	δ^{202}Hg (‰)	Δ^{199}Hg (‰)	Δ^{200}Hg (‰)	Δ^{201}Hg (‰)	References
Zengying, Fujian, China	Mangrove wetland	−1.29 ± 0.33	−0.14 ± 0.03	0.00 ± 0.01	−0.15 ± 0.03	This study
	(Depth of 0 −8 cm)	−1.46 ± 0.14	−0.13 ± 0.02	0.00 ± 0.01	−0.15 ± 0.02	
	(Depth of 8 −16 cm)	−1.05 ± 0.56	−0.13 ± 0.05	0.00 ± 0.01	−0.13 ± 0.06	
	(Depth of 16 −24 cm)	−1.46 ± 0.23	−0.14 ± 0.03	0.00 ± 0.01	−0.16 ± 0.02	
	(Depth of 24 −32 cm)	−1.27 ± 0.22	−0.14 ± 0.04	0.01 ± 0.01	−0.16 ± 0.02	
	(Depth of 32 −40 cm)	−1.22 ± 0.21	−0.14 ± 0.01	0.00 ± 0.01	−0.16 ± 0.02	
Zini, Fujian, China	Mangrove wetland	−0.86 ± 0.25	−0.12 ± 0.03	0.01 ± 0.02	−0.12 ± 0.03	Huang et al., 2020
Shatian, Guangxi, China		−1.55 ± 0.19	−0.22 ± 0.09	0.03 ± 0.06	−0.24 ± 0.09	
Mawei, Guangxi, China	Mangrove wetland	−2.16 ± 0.42	0.09 ± 0.06	0.01 ± 0.02	0.02 ± 0.07	Huang et al., 2022
Fugong, Fujian, China	Mangrove wetland	−0.87 ± 0.05	0.09 ± 0.04		0.01 ± 0.02	Sun et al., 2017
Campos Basin, Rio de Janeiro State, Brazil	Mangrove wetland	−0.96 ± 0.58	−0.11 ± 0.12			Araujo et al., 2017
Hackensack River, New Jersey, USA	River and estuary	−0.38 ± 0.14	0.00 ± 0.03	0.01 ± 0.02	−0.01 ± 0.03	Reinfelder and Janssen, 2019

photoreduction of Hg in natural aquatic environments, respectively (Bergquist and Blum, 2007). The $\Delta^{199}Hg/\delta^{202}Hg$ ratio typically exceeds 1.15 in photo-induced Hg reduction processes, whereas the slope of $\Delta^{199}Hg/\delta^{202}Hg$ is 0 or -0.12 in the microbial reduction and abiotic oxidation of Hg in the dark (Blum et al., 2014). In the present study, the sediment $\Delta^{199}Hg/\Delta^{201}Hg$ ratio was 0.87 ± 0.12 (Pearson's r = 0.97), indicating that the Hg in the study area had undergone photo reduction processes (Figure 4A). Additionally, the sediment $\Delta^{199}Hg/\delta^{202}Hg$ ratio was 0.05 ± 0.01 (Pearson's r = 0.58), suggesting that biotic or abiotic redox processes in the absence of light are also significant biochemical pathways for Hg (Figure 4B).

In addition to THg and MeHg, the Hg isotopic parameters demonstrated significant associations with biogenic elements in sediments, particularly with TOC. For instance, $\delta^{202}Hg$ showed an inverse relationship with TOC (Pearson's r = -0.35), whereas $\Delta^{201}Hg$ showed a positive correlation with both TOC (Pearson's r = 0.481) and TN (Pearson's r = 0.41). These associations imply that elucidating the origin of organic matter in sediments can improve our understanding of Hg migration. The organic matter present in mangrove ecosystems may stem from both internal sources (such as litter and root detritus) and external sources (such as riverine and tidal inputs) (Yu et al., 2012). The C/N ratio serves as a commonly employed indicator of the origin of organic matter within sedimentary environments, given the distinct C/N ratios associated with organic matter derived from various sources.

Marine algae are generally high in proteins and low in cellulose, resulting in a C/N ratio typically ranging from 3 to 8. In contrast, terrestrial vascular plants are characterized by a high cellulose content and a low protein content, with a C/N ratio of 20 or higher. A greater C/N ratio in sediment corresponds to a larger proportion of allochthonous organic matter. A C/N ratio greater than 10 in sediment samples suggests that the organic matter present is predominantly derived from allochthonous sources, whereas a C/N ratio below 10 suggests that the organic matter is primarily from autochthonous sources. A C/N ratio of approximately 10 indicates a balance between autochthonous and allochthonous organic matter (Krishnamurthy et al., 1986). The sediment samples collected from the study site consistently exhibited a C/N ratio exceeding 10, with a median value of 17.08. This suggests that the organic carbon in the mangrove sediments was primarily sourced from terrestrial pollution and higher plant materials, with a small contribution from phytoplankton. This indicates that within the study area, a coastal wetland near an urban center, a significant portion of mangrove litter remains within the site rather than being carried into the bay by seawater. Furthermore, pollutants from terrestrial sources entering the sea via runoff are probably transported to and deposited within the study site due to tidal influences. Consequently, it can be inferred that the pollution inputs in the study area from both seaward and landward directions are comparable and predominantly from terrestrial sources. Thus, the THg distribution pattern in the sediments, with higher concentrations near both the landward and the seaward side compared to the middle section, along with the absence of significant differences in Hg isotopic characteristics, may be explained by a common pathway of organic matter accumulation in the sediments. Specifically, it is probable that anthropogenic Hg inputs from the land migrate and enter the study site through both the landward and seaward sides. Moreover, the decline of sedimentary TOC, TN, and THg concentrations with depth provides additional evidence that the biogenic elements and Hg in the sediments are likely the result of external inputs. Research has indicated that elevated salinity levels can result in the breakdown or aggregation and settling of high-molecular-weight organic substances linked to Hg, ultimately resulting in the discharge of Hg into the aquatic environment (Cavalcante et al., 2024). Nevertheless, the findings of this study suggest that this mechanism is not currently capable of counteracting the buildup of externally introduced Hg and biogenic elements at the locations where samples were collected.

4.3 Impacts of SLR

A rise in sea level can have substantial effects on the organic carbon (OC) content and storage within mangrove forest soils. Given their status as some of the most productive terrestrial forest ecosystems in the world, alterations in the capacity of carbon sequestration in mangrove wetlands will have considerable implications for global carbon cycling and storage (Chen et al., 2020). In this study, the two neighboring areas in which mangrove

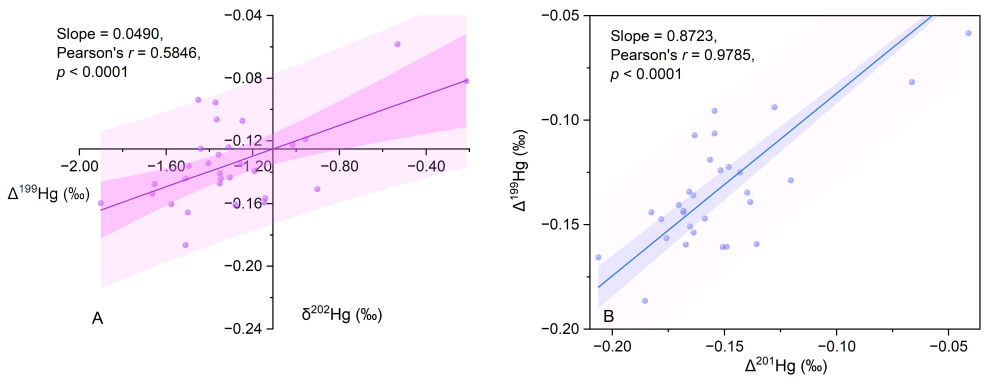

FIGURE 4
Mercury isotopic signatures and correlations. **(A)** $\Delta^{199}Hg$ versus $\delta^{202}Hg$ in sediment samples; **(B)** $\Delta^{201}Hg$ versus $\Delta^{199}Hg$ in sediment samples.

plants (*Kandelia candel*) are cultivated at varying elevations present optimal settings for examining the effects of rising sea levels on mangrove attributes. Recent investigations carried out at our research site have revealed that as sea levels increase, mangroves have shown an enhanced capacity to enhance soil organic carbon levels (Chen et al., 2020). However, there has been a discernible decline in both vegetation biomass and organic carbon storage within mangroves (Chen et al., 2022). The TOC content in sediments at the lower-elevation site (SLR 40 cm) with extended inundation periods was marginally higher compared to that of the SLR 0 cm site, whereas the TN and TP levels were significantly higher at the SLR 40 cm site. This suggests that SLR will enhance nutrient retention in sediments within mangrove wetlands. Previous studies have demonstrated that SLR results in heightened inundation depths and prolonged flooding periods in coastal wetlands, which may decrease soil bulk density (Wang et al., 2019) and impede the microbially mediated degradation of organic material (Breithaupt et al., 2012), consequently fostering the accumulation of organic matter in mangrove soils (Chen et al., 2020).

Most Hg found in estuarine and nearshore sediments is bound to organic matter, with available sites on the organic matter for further Hg adsorption (Chakraborty et al., 2014). This indicates that in addition to the introduction of Hg by organic matter, the organic matter present in sediments can also enhance Hg retention from the surrounding environment. Due to the strong association between Hg and organic carbon, fluctuations in wetland water levels can impact the dispersion and movement of Hg within wetland sediments. The concentrations of THg and MeHg were elevated in the mangrove wetland sediments at the SLR 40 cm site compared to the SLR 0 cm site, suggesting that prolonged inundation enhances the capacity of these sediments to sequester Hg. This phenomenon is commonly linked to the negative correlation between SLR and oxygen diffusion rates (Hickey et al., 2018). Extended inundation not only physically isolates the sediments from the atmosphere but also inhibits the burrowing activities of benthic organisms, thereby reducing the exposed surface area of the sediments. These factors impede the interaction between sediments and atmospheric oxygen, leading to more pronounced reductive conditions within the sediments and an increase in sulfide concentrations resulting from biogeochemical processes (Pan et al., 2023). Given that Hg is predominantly linked to sulfides within the sediments (Crowther et al., 2021), the heightened sulfide levels may promote the transformation of other Hg species, such as soluble divalent Hg ions, into the more stable cinnabar (HgS) within the SLR 40 cm site (Sunderland et al., 2006). This, in turn, enhances the sediments' capacity to sequester Hg (Myrbo et al., 2017). Furthermore, the C/N ratio was notably reduced at the SLR 40 cm site in comparison to the SLR 0 cm site, implying diminished terrestrial pollution influx at the former. Nevertheless, the site at SLR 40 cm showed higher concentrations of THg and MeHg, suggesting that despite lower mercury deposition through sedimentation, the lower-elevation site had a greater capacity for adsorbing environmental Hg compared to the SLR 0 m site. This may be attributed to the stronger binding of Hg at lower elevations due to the availability of more sulfides.

In addition to the presence of THg, the methylation level in sediments is influenced by their physicochemical properties (Zhao et al., 2020). Microbial methylation can be enhanced, albeit within a specific range, by a reduction in the surface sediment oxygen content (Fitzgerald et al., 2007). In areas experiencing longer inundation periods, such as the SLR 40 cm area, the lower surface sediment oxygen content may lead to increased microbial methylation and higher levels of MeHg in the sediments. This finding is consistent with previous results regarding the effects of low-oxygen or anoxic sediment conditions on Hg methylation (Emili et al., 2011).

At the SLR 0 m site, the shorter inundation period may result in extended light exposure and heightened diurnal temperature variations. These conditions can enhance the photoreduction of Hg and the photodegradation of MeHg, thereby facilitating the reduction and emission of accumulated Hg in surface sediments into the atmosphere (Ye et al., 2020), which ultimately leads to increased Hg losses compared to the SLR 40 m site. Nevertheless, SLR may also inhibit the growth of wetland vegetation and a reduction in plant biomass. Data collected in 2017 from the same site indicate that the plant density in the SLR 40 cm area (2.75 ± 0.54 plants/m^2) was significantly lower than that in the SLR 0 cm area (4.08 ± 0.51 plants/m^2), and the average canopy width in the SLR 40 cm area (46.41 ± 9.00 cm) was smaller compared to that in the SLR 0 cm area (> 60 cm) (Chen et al., 2022). Whilst the difference in canopy cover may impact light intensity at the surface and the release of surface Hg, it is not the primary factor contributing to the differences in Hg sequestration among the sites with different elevations.

The Δ^{201}Hg value at the SLR 40 m site showed a slight decrease compared to that at the SLR 0 m site, contrary to the trend observed for THg. Across the sites, there was a significant positive correlation between Δ^{201}Hg and THg concentrations. This apparent contradiction may be attributed to the higher light exposure at the elevated site, resulting in photoreduction of Hg(II) and the photodegradation of MeHg, leading to positive MIF and an increase in the Δ^{201}Hg value (Bergquist and Blum, 2007). In contrast, the low-light SLR 0 m site may present an increased potential for Hg(II) reduction processes facilitated by soluble organic matter in the absence of light, potentially resulting in negative MIF (Zheng and Hintelmann, 2010). Consequently, the observed disparity in Δ^{201}Hg between the SLR 40 m and SLR 0 m sites can be attributed to MIF phenomena occurring within the respective sites. However, this discrepancy is not evident in other Hg isotopic compositions, indicating the necessity for more extensive and prolonged analyses to substantiate these findings.

5 Conclusion

Mercury accumulation was observed in the sediments of the artificial mangrove wetland in Zengying, which is characterized by a low pollution level. The region remains in a state of Hg input, continuously exerting its function as a Hg sink. The primary source of Hg in the plots is represented by anthropogenic emissions from the surrounding land, entering the wetland from both landward and seaward directions. This underscores the significance of mangrove

restoration in mitigating Hg pollution in coastal ecosystems and the influence of anthropogenic Hg emissions on marine environments. The accumulation of Hg in mangrove wetlands is in line with the accumulation of biogenic elements. Higher concentrations of Hg and biogenic elements were found in the sediments of low-elevation plots compared to high-elevation ones, suggesting that SLR has a substantial impact on the wetland's ability to store Hg and influence the biogeochemical cycling of this element in the environment.

Data availability statement

The original contributions presented in the study are included in the article/Supplementary Material. Further inquiries can be directed to the corresponding author.

Author contributions

XY: Data curation, Writing – review & editing, Writing – original draft, Investigation. LS: Supervision, Writing – review & editing, Writing – original draft, Methodology, Data curation. XC: Writing – original draft, Methodology, Investigation, Data curation. YL: Writing – original draft, Investigation, Data curation. JZ: Writing – original draft, Investigation, Data curation. DY: Writing – review & editing, Supervision, Resources, Project administration, Funding acquisition. JW: Writing – review & editing, Investigation, Data curation. SS: Writing – review & editing, Data curation.

Funding

The author(s) declare financial support was received for the research, authorship, and/or publication of this article. This study was funded by the Natural Science Foundation of China (No.41406120), the Natural Science Foundation of Xiamen, China (No. 3502Z20227320), and the Natural Science Foundation of Zhangzhou, China (No. ZZ2023J17).

Acknowledgments

We thank the reviewers for their constructive comments and suggestions. We are also indebted to Dr. Chen Yaojin for her assistance in using MC-ICP-MS.

Conflict of interest

The authors declare that the research was conducted in the absence of any commercial or financial relationships that could be construed as a potential conflict of interest.

Publisher's note

All claims expressed in this article are solely those of the authors and do not necessarily represent those of their affiliated organizations, or those of the publisher, the editors and the reviewers. Any product that may be evaluated in this article, or claim that may be made by its manufacturer, is not guaranteed or endorsed by the publisher.

Supplementary material

The Supplementary Material for this article can be found online at: https://www.frontiersin.org/articles/10.3389/fmars.2024.1444302/full#supplementary-material

References

Albert, S., Saunders, M. I., Roelfsema, C. M., Leon, J. X., Johnstone, E., Mackenzie, J. R., et al. (2017). Winners and losers as mangrove, coral and seagrass ecosystems respond to sea-level rise in Solomon Islands. *Environ. Res. Lett.* 12. doi: 10.1088/1748-9326/aa7e68

Al Sulaiti, M. M., Soubra, L., and Al Ghouti, M. A. (2022). The causes and effects of mercury and methylmercury contamination in the marine environment: A review. *Curr. pollut. Re.* 8, 249–272. doi: 10.1007/s40726-022-00226-7

Amos, H. M., Jacob, D. J., Streets, D. G., and Sunderland, E. M. (2013). Legacy impacts of all-time anthropogenic emissions on the global mercury cycle. *Glob. Biogeochem. Cycle* 27, 410–421. doi: 10.1002/gbc.20040

Araujo, B. F., Hintelmann, H., Dimock, B., Almeida, M. G., and Rezende, C. E. (2017). Concentrations and isotope ratios of mercury in sediments from shelf and continental slope at Campos Basin near Rio de Janeiro, Brazil. *Chemosphere* 178, 42–50. doi: 10.1016/j.chemosphere.2017.03.056

Ariya, P. A., Amyot, M., Dastoor, A., Deeds, D., Feinberg, A., Kos, G., et al. (2015). Mercury physicochemical and biogeochemical transformation in the atmosphere and at atmospheric interfaces: A review and future directions. *Chem. Rev.* 115, 3760–3802. doi: 10.1021/cr500667e

Beckers, F., and Rinklebe, J. (2017). Cycling of mercury in the environment: Sources, fate, and human health implications: A review. *Crit. Rev. Environ. Sci. Technol.* 47, 693–794. doi: 10.1080/10643389.2017.1326277

Bergamaschi, B. A., Fleck, J. A., Downing, B. D., Boss, E., Pellerin, B. A., and Ganju, N. K. (2012a). Mercury dynamics in a San Francisco estuary tidal wetland: Assessing dynamics using *in situ* measurements. *Estuar. Coast.* 35, 1036–1048. doi: 10.1007/s12237-012-9501-3

Bergamaschi, B. A., Krabbenhoft, D. P., Aiken, G. R., Patino, E., Rumbold, D. G., and Orem, W. H. (2012b). Tidally driven export of dissolved organic carbon, total mercury, and methylmercury from a mangrove-dominated estuary. *Environ. Sci. Technol.* 46, 1371–1378. doi: 10.1021/es2029137

Bergquist, B. A., and Blum, J. D. (2007). Mass-dependent and -independent fractionation of Hg isotopes by photoreduction in aquatic systems. *Science* 318, 417–420. doi: 10.1126/science.1148050

Blum, J. D., Sherman, L. S., and Johnson, M. W. (2014). Mercury isotopes in Earth and environmental sciences. *Annu. Rev. Earth Pl. Sci.* 42, 249–269. doi: 10.1146/annurev-earth-050212-124107

Bouchet, S., Tessier, E., Monperrus, M., Bridou, R., Clavier, J., Thouzeau, G., et al. (2011). Measurements of gaseous mercury exchanges at the sediment-water, water-atmosphere and sediment-atmosphere interfaces of a tidal environment (Arcachon Bay, France). *J. Environ. Monit.* 13, 1351–1359. doi: 10.1039/c0em00358a

Breithaupt, J. L., Smoak, J. M., Iii, T. J. S., Saunders, C. J., and Hoare, A. (2012). Organic carbon burial rates in mangrove sediments: Strengthening the global budget. *Glob. Biogeochem. Cycle* 26. doi: 10.1029/2012GB004375

Cai, L. M., Wang, Q. S., Wen, H. H., Luo, J., and Wang, S. (2019). Heavy metals in agricultural soils from a typical township in Guangdong Province, China: Occurrences and spatial distribution. *Ecotox. Environ. Safe.* 168, 184–191. doi: 10.1016/j.ecoenv.2018.10.092

Castro, S., Luiz Silva, W., MaChado, W., and Valezio, E. (2021). Mangrove sediments as long-term mercury sinks: Evidence from millennial to decadal time scales. *Mar. pollut. Bull.* 173. doi: 10.1016/j.marpolbul.2021.113031

Cavalcante, M. S., Marins, R. V., and Mounier, S. (2024). Non-conservative behavior of organic matter and its interaction with metals in an equatorial estuary, Brazil. *Environ. Sci. pollut. Res.* 31, 34309–34323. doi: 10.1007/s11356-024-33521-5

Chai, M., Li, R., Qiu, Z., Niu, Z., and Shen, X. (2020). Mercury distribution and transfer in sediment-mangrove system in urban mangroves of fast-developing coastal region; southern China. *Estuar. Coast. Shelf. Sci.* 240. doi: 10.1016/j.ecss.2020.106770

Chakraborty, P., Sharma, B., Babu, P. V. R., Yao, K. M., and Jaychandran, S. (2014). Impact of total organic carbon (in sediments) and dissolved organic carbon (in overlying water column) on Hg sequestration by coastal sediments from the central east coast of India. *Mar. pollut. Bull.* 79, 342–347. doi: 10.1016/j.marpolbul.2013.11.028

Chen, J., Gao, M., Chen, G., Zhu, H., and Ye, Y. (2022). Biomass accumulation and organic carbon stocks of Kandelia obovata mangrove vegetation under different simulated sea levels. *Acta Oceanol. Sin.* 41, 78–86. doi: 10.1007/s13131-021-1891-2

Chen, J., Huang, Y., Chen, G., and Ye, Y. (2020). Effects of simulated sea level rise on stocks and sources of soil organic carbon in Kandelia obovata mangrove forests. *For. Ecol. Manag.* 460. doi: 10.1016/j.foreco.2020.117898

Chen, Y. P., and Ye, Y. (2014). Early responses of Avicennia marina (Forsk.) Vierh. to intertidal elevation and light level. *Aquat. Bot.* 112, 33–40. doi: 10.1016/j.aquabot.2013.07.006

Correia, R. R. S., and Guimaraes, J. R. D. (2017). Mercury methylation and sulfate reduction rates in mangrove sediments, Rio de Janeiro, Brazil: The role of different microorganism consortia. *Chemosphere* 167, 438–443. doi: 10.1016/j.chemosphere.2016.09.153

Crowther, E. R., Demers, J. D., Blum, J. D., Brooks, S. C., and Johnson, M. W. (2021). Use of sequential extraction and mercury stable isotope analysis to assess remobilization of sediment-bound legacy mercury. *Environ. Sci-Proc. Imp.* 23, 756–775. doi: 10.1039/D1EM00019E

da Silva, F. S., Pereira, D. D., Nuñez, L. S., Krepsk, N., Fontana, L. F., Baptista, J. A., et al. (2008). Bacteriological study of the superficial sediments of Guanabara Bay, RJ, Brazil. *Braz. J. Oceanogr.* 56, 13–22. doi: 10.1590/S1679-87592008000100002

Dastoor, A., Angot, H., Bieser, J., Christensen, J. H., Douglas, T. A., Heimbürger Boavida, L. E., et al. (2022). Arctic mercury cycling. *Nat. Rev. Earth Environ.* 3, 270–286. doi: 10.1038/s43017-022-00269-w

de Lacerda, L. D., Marins, R. V., and Dias, F. J. D. (2020). An arctic paradox: Response of fluvial Hg inputs and bioavailability to global climate change in an extreme coastal environment. *Front. Earth Sci.* 8. doi: 10.3389/feart.2020.00093

de Lacerda, L. D., Ward, R. D., Borges, R., and Ferreira, A. C. (2022). Mangrove trace metal biogeochemistry response to global climate change. *Front. For. Glob. Chang* 5. doi: 10.3389/ffgc.2022.817992

De Pontes, G. C., Vicente, M. D. C., Kasper, D., MaChado, W. T., and Wasserman, J. C. (2023). Spatial distribution of total mercury and methylmercury in the sediment of a tropical coastal environment subjected to heavy urban inputs. *Chemosphere* 312. doi: 10.1016/j.chemosphere.2022.137067

Duan, D. D., Lei, P., Lan, W. L., Li, T. S., Zhang, H., Zhong, H., et al. (2021). Litterfall-derived organic matter enhances mercury methylation in mangrove sediments of south China. *Sci. Total. Environ.* 765. doi: 10.1016/j.scitotenv.2020.142763

Dutton, A., Carlson, A. E., Long, A. J., Milne, G. A., Clark, P. U., DeConto, R., et al. (2015). Sea-level rise due to polar ice-sheet mass loss during past warm periods. *Science* 349. doi: 10.1126/science.aaa4019

Emili, A., Koron, N., Covelli, S., Faganeli, J., Acquavita, A., Predonzani, S., et al. (2011). Does anoxia affect mercury cycling at the sediment-water interface in the Gulf of Trieste (northern Adriatic Sea)? Incubation experiments using benthic flux chambers. *Appl. Geochem.* 26, 194–204. doi: 10.1016/j.apgeochem.2010.11.019

Estrade, N., Carignan, J., and Donard, O. F. X. (2011). Tracing and quantifying anthropogenic mercury sources in soils of northern France using isotopic signatures. *Environ. Sci. Technol.* 45, 1235–1242. doi: 10.1021/es1026823

Feng, P. Y., Xiang, Y. P., Cao, D., Li, H., Wang, L. Q., Wang, M. X., et al. (2022). Occurrence of methylmercury in aerobic environments: Evidence of mercury bacterial methylation based on simulation experiments. *J. Hazard. Mater.* 438. doi: 10.1016/j.jhazmat.2022.129560

Fitzgerald, W. F., Lamborg, C. H., and Hammerschmidt, C. R. (2007). Marine biogeochemical cycling of mercury. *Chem. Rev.* 107, 641–662. doi: 10.1021/cr050353m

Gehrke, G. E., Blum, J. D., and Meyers, P. A. (2007). The geochemical behavior and isotopic composition of Hg in a mid-Pleistocene western Mediterranean sapropel. *Geochim. Cosmochim. Acta* 73, 1651–1665. doi: 10.1016/j.gca.2008.12.012

Gonzalez Raymat, H., Liu, G., Liriano, C., Li, Y., Yin, Y., Shi, J., et al. (2017). Elemental mercury: Its unique properties affect its behavior and fate in the environment. *Environ. pollut.* 229, 69–86. doi: 10.1016/j.envpol.2017.04.101

Guimaraes, J. R. D., Meili, M., Hylander, L. D., Silva, E. D. E., Roulet, M., Mauro, J. B. N., et al. (2000). Mercury net methylation in five tropical flood plain regions of Brazil: high in the root zone of floating macrophyte mats but low in surface sediments and flooded soils. *Sci. Total. Environ.* 261, 99–107. doi: 10.1016/S0048-9697(00)00628-8

Hickey, S. M., Callow, N. J., Phinn, S., Lovelock, C. E., and Duarte, C. M. (2018). Spatial complexities in aboveground carbon stocks of a semi-arid mangrove community: A remote sensing height-biomass-carbon approach. *Estuar. Coast. Shelf. Sci.* 200, 194–201. doi: 10.1016/j.ecss.2017.11.004

Huang, S., Jiang, R., Song, Q., Zhang, Y., Huang, Q., Su, B., et al. (2020). Study of mercury transport and transformation in mangrove forests using stable mercury isotopes. *Sci. Total. Environ.* 704. doi: 10.1016/j.scitotenv.2019.135928

Huang, S., Jiang, R., Song, Q., Zhao, Y., Lv, S., Zhang, Y., et al. (2022). The Hg behaviors in mangrove ecosystems revealed by Hg stable isotopes: a case study of Maowei mangrove. *Environ. Sci. pollut. Res.* 29, 25349–25359. doi: 10.1007/s11356-021-17744-4

Islam, M. A., Al-mamun, A., Hossain, F., Quraishi, S. B., Naher, K., Khan, R., et al. (2017). Contamination and ecological risk assessment of trace elements in sediments of the rivers of Sundarban mangrove forest, Bangladesh. *Mar. pollut. Bull.* 124, 356–366. doi: 10.1016/j.marpolbul.2017.07.059

Johnson, N. W., Mitchell, C. P. J., Engstrom, D. R., Bailey, L. T., Coleman Wasik, J. K., and Berndt, M. E. (2016). Methylmercury production in a chronically sulfate-impacted sub-boreal wetland. *Environ. Sci-Proc. Imp.* 18, 725–734. doi: 10.1039/C6EM00138F

Krishnamurthy, R. V., Bhattacharya, S. K., and Kusumgar, S. (1986). Palaeoclimatic changes deduced from 13C/12C and C/N ratios of Karewa lake sediments, India. *Nature* 323, 150–152. doi: 10.1038/323150a0

Kristensen, E., Bouillon, S., Dittmar, T., and Marchand, C. (2008). Organic carbon dynamics in mangrove ecosystems: A review. *Aquat. Bot.* 89, 201–219. doi: 10.1016/j.aquabot.2007.12.005

Kurz, A. Y., Blum, J. D., Washburn, S. J., and Baskaran, M. (2019). Changes in the mercury isotopic composition of sediments from a remote alpine lake in Wyoming, USA. *Sci. Total. Environ.* 669, 973–982. doi: 10.1016/j.scitotenv.2019.03.165

Lei, P., Zhong, H., Duan, D. D., and Pan, K. (2019). A review onmercury biogeochemistry inmangrove sediments: Hotspots of methylmercury production? *Sci. Total. Environ.* 680, 140–150. doi: 10.1016/j.scitotenv.2019.04.451

Li, R. L., Xu, H. L., Chai, M. W., and Qiu, G. Y. (2016). Distribution and accumulation of mercury and copper in mangrove sediments in Shenzhen, the world's most rapid urbanized city. *Environ. Monit. Assess.* 188. doi: 10.1007/s10661-016-5103-z

Lin, H., Yuan, D., Lu, B., Huang, S., Sun, L., Zhang, F., et al. (2015). Isotopic composition analysis of dissolved mercury in seawater with purge and trap preconcentration and a modified Hg introduction device for MC-ICP-MS. *J. Anal. Atom. Spectrom.* 30, 353–359. doi: 10.1039/C4JA00242C

Liu, N., Cai, X., Jia, L., Wang, X., Yuan, W., Lin, C. J., et al. (2023). Quantifying mercury distribution and source contribution in surface soil of Qinghai-Tibetan Plateau using mercury isotopes. *Environ. Sci. Technol.* 57, 5903–5912. doi: 10.1021/acs.est.2c09610

Liu, M., Zhang, Q., Cheng, M., He, Y., Chen, L., Zhang, H., et al. (2019). Rice life cycle-based global mercury biotransport and human methylmercury exposure. *Nat. Commun.* 10. doi: 10.1038/s41467-019-13221-2

Lovelock, C. E., and Ellison, J. (2007). Great Barrier Reef Marine Park Authority ch. 9 (DAFF). Australia. ch. 9. Available at: http://www.daff.gov.au/fisheries/environment/sharks/sharkplan2/s.

Luo, Y., Duan, L., Driscoll, C. T., Xu, G. Y., Shao, M. S., Taylor, M., et al. (2016). Foliage-atmosphere exchange of mercury in a subtropical coniferous forest in south China. *J. Geophys. Res-Biogeo.* 121, 2006–2016. doi: 10.1002/2016JG003388

Ma, M., Du, H. X., and Wang, D. Y. (2019). Mercury methylation by anaerobic microorganisms: A review. *Crit. Rev. Environ. Sci. Technol.* 49, 1893–1936. doi: 10.1080/10643389.2019.1594517

Mao, L. L., Liu, X. T., Wang, B. D., Lin, C. Y., Xin, M., Zhang, B. T., et al. (2020). Occurrence and risk assessment of total mercury and methylmercury in surface seawater and sediments from the Jiaozhou Bay, Yellow Sea. *Sci. Total. Environ.* 714, 13. doi: 10.1016/j.scitotenv.2020.136539

Meng, B., Li, Y. B., Cui, W. B., Jiang, P., Liu, G. L., Wang, Y. M., et al. (2018). Tracing the uptake, transport, and fate of mercury in sawgrass (cladium jamaicense) in the Florida everglades using a multi-isotope technique. *Environ. Sci. Technol.* 52, 3384–3391. doi: 10.1021/acs.est.7b04150

Mikac, N., Picer, M., Stegnar, P., and Tusekznidaric, M. (1985). Mercury distribution in a polluted marine area, ratio of total mercury, methyl mercury and selenium in sediments, mussels and fish. *Water Res.* 19, 1387–1392. doi: 10.1016/0043-1354(85)90305-7

Moreau, J. W., Gionfriddo, C. M., Krabbenhoft, D. P., Ogorek, J. M., DeWild, J. F., Aiken, G. R., et al. (2015). The effect of natural organic matter on mercury methylation by Desulfobulbus propionicus 1pr3. *Front. Microbiol.* 6. doi: 10.3389/fmicb.2015.01389

Myrbo, A., Swain, E. B., Johnson, N. W., Engstrom, D. R., Pastor, J., Dewey, B., et al. (2017). Increase in nutrients, mercury, and methylmercury as a consequence of elevated sulfate reduction to sulfide in experimental wetland mesocosms. *J. Geophys. Res-Biogeo.* 122, 2769–2785. doi: 10.1002/2017JG003788

Navya, C., Gopikrishna, V. G., Arunbabu, V., and Mohan, M. (2015). Distribution and fractionation of mercury in the soils of a unique tropical agricultural wetland

ecosystem, southwest coast of India. *Environ. Monit. Assess.* 187, 11. doi: 10.1007/s10661-015-4972-x

Neal Walthall, N., Ndu, U., Rivera, N. A., Elias, D. A., and Hsu Kim, H. (2022). Utility of diffusive gradient in thin-film passive samplers for predicting mercury methylation potential and bioaccumulation in freshwater wetlands. *Environ. Sci. Technol.* 56, 1743–1752. doi: 10.1021/acs.est.1c06796

Obrist, D., Johnson, D. W., and Edmonds, R. L. (2012). Effects of vegetation type on mercury concentrations and pools in two adjacent coniferous and deciduous forests. *J. Plant Nutr. Soil Sci.* 175, 68–77. doi: 10.1002/jpln.201000415

Pan, F., Xiao, K., Cai, Y., Li, H. L., Guo, Z. R., Wang, X. H., et al. (2023). Integrated effects of bioturbation, warming and sea-level rise on mobility of sulfide and metalloids in sediment porewater of mangrove wetlands. *Water. Res.* 233. doi: 10.1016/j.watres.2023.119788

Passos, T., Penny, D., Barcellos, R., Nandan, S. B., Babu, D. S. S., Santos, I. R., et al. (2022). Increasing carbon, nutrient and trace metal accumulation driven by development in a mangrove estuary in south Asia. *Sci. Total. Environ.* 832. doi: 10.1016/j.scitotenv.2022.154900

Poulain, A. J., Garcia, E., Amyot, M., Campbell, P. G. C., Raofie, F., and Ariya, P. A. (2007). Biological and chemical redox transformations of mercury in fresh and salt waters of the high arctic during Spring and Summer. *Environ. Sci. Technol.* 41, 1883–1888. doi: 10.1021/es061980b

Poulin, B. A., Ryan, J. N., Tate, M. T., Krabbenhoft, D. P., Hines, M. E., Barkay, T., et al. (2019). Geochemical factors controlling dissolved elemental mercury and methylmercury formation in Alaskan wetlands of varying trophic status. *Environ. Sci. Techol.* 53, 6203–6213. doi: 10.1021/acs.est.8b06041

Regnell, O., and Watras, C. J. (2019). Microbial mercury methylation in aquatic environments: A critical review of published field and laboratory studies. *Environ. Sci. Technol.* 53, 4–19. doi: 10.1021/acs.est.8b02709

Reinfelder, J. R., and Janssen, S. E. (2019). Tracking legacy mercury in the Hackensack River estuary using mercury stable isotopes. *J. Hazard. Mater.* 375, 121–129. doi: 10.1016/j.jhazmat.2019.04.074

Saintilan, N., Khan, N. S., Ashe, E., Kelleway, J. J., Rogers, K., Woodroffe, C. D., et al. (2020). Thresholds of mangrove survival under rapid sea level rise. *Science* 368, 1118–1121. doi: 10.1126/science.aba2656

Selvendiran, P., Driscoll, C. T., Montesdeoca, M. R., and Bushey, J. T. (2008). Inputs, storage, and transport of total and methyl mercury in two temperate forest wetlands. *J. Geo. Res-Biogeo.* 113. doi: 10.1029/2008JG000739

Siau, Y. F., Le, D. Q., Suratman, S., Jaaman, S. A., Tanaka, K., and Kotaro, S. (2021). Seasonal variation of total mercury transfer through a tropical mangrove food web, Setiu Wetlands. *Mar. pollut. Bull.* 162, 111878. doi: 10.1016/j.marpolbul.2020.111878

Sun, L., Lu, B., Yuan, D., Hao, W., and Zheng, Y. (2017). Variations in the isotopic composition of stable mercury isotopes in typical mangrove plants of the Jiulong estuary, SE China. *Environ. Sci. pollut. Res.* 24, 1459–1468. doi: 10.1007/s11356-016-7933-1

Sunderland, E. M., Gobas, F., Branfireun, B. A., and Heyes, A. (2006). Environmental controls on the speciation and distribution of mercury in coastal sediments. *Mar. Chem.* 102, 111–123. doi: 10.1016/j.marchem.2005.09.019

Tang, W. L., Liu, Y. R., Guan, W. Y., Zhong, H., Qu, X. M., and Zhang, T. (2020). Understanding mercury methylation in the changing environment: Recent advances in assessing microbial methylators and mercury bioavailability. *Sci. Total. Environ.* 714. doi: 10.1016/j.scitotenv.2020.136827

Teixeira, D. C., Lacerda, L. D., and Silva-Filho, E. V. (2017). Mercury sequestration by rainforests: The influence of microclimate and different successional stages. *Chemosphere* 168, 1186–1193. doi: 10.1016/j.chemosphere.2016.10.081

Teixeira, D. C., Lacerda, L. D., and Silva-Filho, E. V. (2018). Foliar mercury content from tropical trees and its correlation with physiological parameters *in situ*. Environ. *Pollut* 242, 1050–1057. doi: 10.1016/j.envpol.2018.07.120

Thibodeau, A. M., and Bergquist, B. A. (2017). Do mercury isotopes record the signature of massive volcanism in marine sedimentary records? *Geology* 45, 95–96. doi: 10.1130/focus012017.1

Thompson Roberts, E. S., and Pick, F. R. (2000). Total mercury in the water and sediments of St. Lawrence River wetlands compared with inland wetlands of Temagami North Bay and Muskoka-Haliburton. *Can. J. Fish. Aquat. Sci.* 57, 148–154. doi: 10.1139/cjfas-57-S1-148

Tjerngren, I., Meili, M., Bjorn, E., and Skyllberg, U. (2012). Eight boreal wetlands as sources and sinks for methyl mercury in relation to soil acidity, C/N ratio, and small-scale flooding. *Environ. Sci. Technol.* 46, 8052–8060. doi: 10.1021/es300845x

USEPA (2001). *Methyl mercury in water by distillation, aqueous ethylation, purge and trap, and CVAFS, Method 1630* (Washington, DC: United States Environmental Protection Agency), p54.

USEPA (2002). *Mercury in water by oxidation, purge and trap, and cold vapour atomic fluorescence spectrometry. Method 1631, revision E* (Washington, DC: United States Environmental Protection Agency), p17.

Vilhena, M. S. P., Costa, M. L., and Berredo, J. F. (2013). Accumulation and transfer of Hg, As, Se, and other metals in the sediment-vegetation-crab-human food chain in the coastal zone of the northern Brazilian state of Para (Amazonia). *Environ. Geochem. Hlth.* 35, 477–494. doi: 10.1007/s10653-013-9509-z

Wang, F. M., Lu, X. L., Sanders, C. J., and Tang, J. W. (2019). Tidal wetland resilience to sea level rise increases their carbon sequestration capacity in United States. *Nat. Commun.* 10, 11. doi: 10.1038/s41467-019-13800-3

Wang, X., Luo, J., Yin, R., Yuan, W., Lin, C. J., Sommar, J., et al. (2017). Using mercury isotopes to understand mercury accumulation in the montane forest floor of the eastern Tibetan Plateau. *Environ. Sci. Technol.* 51, 801–809. doi: 10.1021/acs.est.6b03806

Wang, T., Yang, G., Du, H., Guo, P., Sun, T., An, S., et al. (2021). Migration characteristics and potential determinants of mercury in long-term decomposing litterfall of two subtropical forests. *Ecotox. Environ. Safe.* 208. doi: 10.1016/j.ecoenv.2020.111402

Wang, B., Yuan, W., Wang, X., Li, K., Lin, C. J., Li, P., et al. (2022). Canopy-level flux and vertical gradients of Hg-0 stable isotopes in remote evergreen broadleaf forest show year-around net Hg-0 deposition. *Environ. Sci. Technol.* 56, 5950–5959. doi: 10.1021/acs.est.2c00778

Woodroffe, C. D. (1995). Response of tide-dominated mangrove shorelines in northern Australia to anticipated sea-level rise. *Earth Surf. Proc. Land.* 20, 65–85. doi: 10.1002/esp.3290200107

Ye, X. Y., Rountos, K. J., Lee, C. S., and Fisher, N. S. (2021). Effects of methylmercury on the early life stages of an estuarine forage fish using two different dietary sources. *Mar. Environ. Res.* 164. doi: 10.1016/j.marenvres.2020.105240

Ye, Y. T., Sun, L. M., Zhou, L., Lu, C. Y., Yao, Y., and Chen, W. J. (2020). Mercury release flux and its influencing factors from urban tidal flat of young Kandelia candel plantation. *Chin. J. Echol.* 39, 3817–3828. doi: 10.13292/j.1000-4890.202011.006

Yin, R., Feng, X., Li, X., Yu, B., and Du, B. (2014). Trends and advances in mercury stable isotopes as a geochemical tracer. *Trends Environ. Anal. Chem.* 2, 1–10. doi: 10.1016/j.teac.2014.03.001

Yin, R., Guo, Z., Hu, L., Liu, W., Hurley, J. P., Lepak, R. F., et al. (2018). Mercury inputs to Chinese marginal seas: Impact of industrialization and development of China. *J. Geophys. Res-Oceans.* 123, 5599–5611. doi: 10.1029/2017JC013691

Yu, C., Xiao, W., Xu, Y., Sun, X., Li, M., Lin, H., et al. (2021). Spatial-temporal characteristics of mercury and methylmercury in marine sediment under the combined influences of river input and coastal currents. *Chemosphere* 274. doi: 10.1016/j.chemosphere.2021.129728

Yu, X. Q., Yang, J., Liu, L. M., Tian, Y., Yu, Z., Wang, C., et al. (2012). Spatial variations of biogenic elements in coastal wetland sediments of Jiulong River estuary. *Environ. Sci.* 33, 3739–3747. doi: 10.13227/j.hjkx.2012.11.021

Zhao, K., Bao, K., Yan, Y., Neupane, B., and Gao, C. (2022). Spatial distribution of potentially harmful trace elements and ecological risk assessment in Zhanjiang mangrove wetland, South China. *Mar. pollut. Bull.* 182. doi: 10.1016/j.marpolbul.2022.114033

Zhao, L., Meng, B., and Feng, X. B. (2020). Mercury methylation in rice paddy and accumulation in rice plant: A review. *Ecotox. Environ. Safe.* 195, 9. doi: 10.1016/j.ecoenv.2020.110462

Zheng, W., and Hintelmann, H. (2010). Mass independent isotope fractionation of mercury during its photochemical reduction by low-molecular-weight organic compounds. *Geochim. Cosmochim. Acta* 74, A1224. doi: 10.1021/jp9111348

Zhou, Z. W., Wang, H. L., and Li, Y. B. (2023). Mercury stable isotopes in the ocean: Analytical methods, cycling, and application as tracers. *Sci. Total. Environ.* 874, 13. doi: 10.1016/j.scitotenv.2023.162485

Zillioux, E. J., Porcella, D. B., and Benoit, J. M. (1993). Mercury cycling and effects in fresh-water wetland ecosystems. *Environ. Toxicol. Chem.* 12, 2245. doi: 10.1002/etc.5620121208